Earth and Planetary Science Letters 349–350 (2012) 98–108

Contents lists available at SciVerse ScienceDirect

Earth and Planetary Science Letters

journal homepage: www.elsevier.com/locate/epsl

Letters

Atmospheric impacts and ice core imprints of a methane pulse from clathrates

Josué Bock [a], Patricia Martinerie [a,*], Emmanuel Witrant [b], Jérôme Chappellaz [a]

[a] UJF – Grenoble1/CNRS, Laboratoire de Glaciologie et Géophysique de l'Environnement (LGGE), UMR 5183, 54, rue Molière, B.P. 53, Grenoble F-38041, France
[b] UJF – Grenoble1/CNRS, Grenoble Image Parole Signal Automatique (GIPSA-lab), UMR 5216, B.P. 46, F-38402 St Martin d'Hères, France

ARTICLE INFO

Article history:
Received 17 October 2011
Received in revised form
29 May 2012
Accepted 27 June 2012
Editor: P. DeMenocal
Available online 31 July 2012

Keywords:
methane
greenhouse gas
isotopic ratio
clathrate
firn
ice core

ABSTRACT

In relation to Arctic warming, the possible occurrence of methane hydrate degassing events has attracted an increasing interest in recent years. We evaluate the atmospheric impact of rapid and massive emissions of methane and how they are imprinted in ice core records, by combining for the first time models of atmospheric chemistry and trace gas transport in firn. Different emission characteristics as well as climatic conditions (present, pre-industrial, glacial) are considered. The δ isotopic signatures characterizing stable isotopologues of methane DCH_3 and $^{13}CH_4$ are also analysed.

Our results suggest little effect of clathrate degassing on the main methane oxidant: OH radicals. Due to the relatively short atmospheric lifetime of methane, the simulated clathrate-induced perturbations last for less than a century. This time scale is comparable to or shorter than the duration of air bubble closure in polar ice sheets. As a consequence, rapid methane perturbations in the atmosphere are strongly smoothed in ice core records. This smoothing mostly depends on the snow accumulation rate at the site of ice core drilling. We propose a methodology to identify a potential clathrate degassing event in ice core records. Continuous CH_4 records from high accumulation rate sites could allow to decipher short time scale events. δD of CH_4 should reveal a typical "lying S" shape at high accumulation rate sites, reflecting the combined effects of the clathrate source signature (negative excursion) and subsequent OH fractionation in the atmosphere (positive excursion). The amplitude ratio of the negative and positive δD swings recorded in Greenland and Antarctica under similar accumulation rate conditions could also indicate the latitude of a clathrate degassing event.

1. Introduction

Methane is responsible for about a third of the radiative forcing since pre-industrial times and has the second largest radiative impact after CO_2 (IPCC, 2007). This is related to the strong increase in its atmospheric concentration: by a factor of approximately 2.5 (from about 700 ppbv to 1780 ppbv) since the mid-eighteenth century (Etheridge et al., 1998). Natural methane sources such as wetlands, termites, wild ruminants and biomass burning (see Dlugokencky et al., 2011, for a review), can also vary substantially, as revealed by ice core records of the atmospheric methane budget during glacial–interglacial cycles (e.g., Brook et al., 2000; Loulergue et al., 2008, and references therein). However, reconstructing the past methane budget is difficult, as both sources and sinks may have changed (e.g., Levine et al., 2011a; Weber et al., 2010). Wetlands are currently the main natural methane source but some authors put forward the potential role of other methane sources during past periods.

Methane hydrates are a controversial source (Kennett et al., 2000; Nisbet, 1990, 2002; O'Hara, 2008). Also called clathrates, they lie in oceanic sediments and permafrost (see Archer, 2007; Maslin et al., 2010, for recent reviews). Recent estimates suggest that 7–40×10^5 Tg CH_4 (Buffett and Archer, 2004; Milkov, 2004) are stored as hydrates in the ocean and another 25×10^5 Tg CH_4 (Buffett and Archer, 2004) as free gas in the underlying sediments. This is at least two orders of magnitude larger than the atmospheric methane reservoir (about 5000 Tg at present). Archer et al. (2009) calculated a $21–27 \times 10^5$ Tg CH_4 best estimate of the clathrate CH_4 reservoir including hydrates and free gas below hydrate layers. Methane hydrate reservoirs in permafrost soils, oil–gas fields and mud volcanoes are less well known but considered as smaller than marine reservoirs (Archer, 2007; Etiope and Klusman, 2010; Maslin et al., 2010). Two sources of evidence support the occurrence of catastrophic methane releases from hydrates in the recent past: large scale sediment slope failures and negative anomalies in $\delta^{13}C$ of benthic and/or planktonic foraminifera shells.

* Corresponding author. Tel.: +33 4 76 82 42 14; fax: +33 4 76 82 42 01.
E-mail addresses: bock@lgge.obs.ujf-grenoble.fr (J. Bock), martinerie@lgge.obs.ujf-grenoble.fr (P. Martinerie), emmanuel.witrant@ujf-grenoble.fr (E. Witrant), chappellaz@lgge.obs.ujf-grenoble.fr (J. Chappellaz).

0012-821X/$ - see front matter © 2012 Elsevier B.V. All rights reserved.
http://dx.doi.org/10.1016/j.epsl.2012.06.052

Maslin et al. (2004) made an inventory of dated submarine sediment failures (27 events) in the North Atlantic sector for the last 45 kyr (kilo years). They showed that more than 70% by volume of these landslides occurred during two periods: the Bølling Ållerød (between 15 and 13 kyr BP) and the Preboreal (between 11 and 8 kyr BP), two periods when atmospheric methane concentrations increased rapidly. The Storegga slide (in the Norwegian continental margin) involved the largest volume of sediments for the Preboreal period, but recent studies (Bünz et al., 2003; Paull et al., 2007) suggest that part of them contained no clathrates, thus leading to a smaller amount of methane potentially released (about 2×10^3 Tg CH_4, not including methane dissolved in the sediment pore water, Paull et al., 2007).

As dissolved methane in marine water after a degassing event bears a very negative $\delta^{13}C$ isotopic signature, its following consumption by bacterial metabolism leaves a negative $\delta^{13}C$ anomaly in foraminifera shells. Several authors found anomalous $\delta^{13}C$ signatures in both benthic and planktonic foraminifera at different locations (e.g., Kennett et al., 2000; Maslin et al., 2005; Smith et al., 2001), and interpreted them as resulting from episodic massive hydrate dissociation. Estimates of the amount of methane dissolved in the ocean, which could generate such anomalies, range between 10 and 200 Tg CH_4 (de Garidel-Thoron et al., 2004; Kennett et al., 2000; Prokopenko and Williams, 2004). These methane releases spanned over at least a decade. How much of the escaped methane could have reached the atmosphere, however, remains unknown. As an example, Kessler et al. (2011) conclude that the methane released during the Deepwater Horizon oil spill was entirely consumed by deepwater bacterias. Finally, several studies questioned the hydrate dissociation interpretation of the $\delta^{13}C$ records in sediment cores (Cannariato and Stott, 2004; Stott et al., 2002; Torres et al., 2003) and complementary proxies (e.g., radiocarbon or $\delta^{13}C$ of total organic carbon) are needed (see Uchida et al., 2008; Zeebe, 2007, for recent discussions).

Air bubbles trapped in polar ice provide an almost direct record of atmospheric methane over the last 800 kyr (e.g., Loulergue et al., 2008). Several approaches have been used to investigate the signature of an atmospheric methane pulse from clathrates in ice core records. Thorpe et al. (1996) modelled the atmospheric response to a 4000 Tg methane input in glacial conditions and found that the perturbation would last for about 50 yr. Before being trapped in bubbles, the air slowly diffuses in the firn, from the surface down to the close-off zone. The bubble enclosure also takes place progressively. Hence, fast variations of the atmospheric signal are partly smoothed out. For instance Spahni et al. (2003) compared high-resolution records of the 8200 yr BP CH_4 minimum and inferred a 34–59% attenuation at the low accumulation rate Dome C site with respect to GRIP. Thorpe et al. (1996) represented the smoothing effect as a weighted average. They concluded that an ice core sampling interval of about 300 yrs was too long to detect the simulated methane spike from catastrophic hydrate degassing. Brook et al. (2000) used a similar atmospheric scenario and other hypothetical histories as input to a firn model (Severinghaus et al., 1998) adapted to the GISP2 (Greenland) and Taylor Dome (Antarctica) ice core sites. They concluded that these scenarios are inconsistent with the GISP2 methane record, but that the lower resolution Taylor Dome signal does not entirely rule out a Southern Hemisphere clathrate release. Over the last decade, the increasing number of ice core records with sampling frequencies of a few centuries (e.g., Brook et al., 2005; Flückiger et al., 2002; Loulergue et al., 2008), or even a few years (Schüpbach et al., 2009) or decadal resolution on specific methane events (e.g., Brook et al., 2000; Flückiger et al., 2004; Spahni et al., 2003) rendered the missing of a massive methane emission event increasingly unlikely, at least for the last 50,000 yrs.

Methane hydrates have a specific deuterium isotopic signature (δD_{CH_4}) of about −190‰, versus about −290‰ for mean of other sources (Fischer et al., 2008; Milkov, 2005). Sowers (2006) published the first measurements of δD_{CH_4} in ice cores and used a box model including methane isotopes to compare the measured variations with a theoretical response to methane release from clathrates. He concludes that his dataset, which includes three rapid warming and methane increase events (at 11.5, 14.7 and 38.4 kyr BP), are inconsistent with clathrate emissions. Bock et al. (2010) further exclude clathrates from being the cause of rising CH_4 concentrations at the onset of Dansgaard–Oeschger events 7 and 8. Using $^{14}C_{CH_4}$ measurements in ice, which allow to constrain the fossil fraction of methane sources, Petrenko et al. (2009) conclude that wetland sources were likely responsible for the majority of the Younger Dryas–Preboreal CH_4 rise. The correlation between rapid variations of methane and nitrous oxide (Flückiger et al., 1999, 2004; Sowers et al., 2003; Spahni et al., 2005), another greenhouse gas which has no hydrate source, provides another argument against the clathrate hypothesis (Lambert et al., 2006). In conclusion, no clear evidence of a methane release from clathrates has been found so far in ice core records, but some events might have been missed due to sampling resolution and the smoothing effect of firn.

Here, we further investigate the atmospheric and ice-core responses to an hypothetical methane release from hydrates, using both an atmospheric chemistry model and a model of trace gas transport and trapping in firn. The two minor stable isotopes of methane (DCH_3 and $^{13}CH_4$), which reflect additional aspects of the methane budget, are also simulated for the first time. Multiple model runs are performed in order to test the effects of varying emission characteristics (intensity, duration, and latitude), climate conditions (present, Pre-Industrial Holocene (PIH), and Last Glacial Maximum (LGM)) and gas trapping conditions at five ice-core drilling sites. This leads us to identify the most characteristic signals in ice cores pinpointing the signature of a massive methane release from hydrates.

2. Models description

2.1. The atmospheric chemistry model

We use the global two-dimensional (zonally averaged) chemistry-transport-radiation model of Brasseur et al. (1990) and Martinerie et al. (1995). It extends from the Earth surface to 85 km altitude. The time step is 15 days. The model has been updated recently, especially

Table 1
Methane budget for the three simulated periods: present (ACT), Pre-Industrial Holocene (PIH) and Last Glacial Maximum (LGM). The atmospheric isotopic signatures $\delta^{13}C_{CH_4}$ and δD_{CH_4} were derived from Fischer et al. (2008) and Sowers (2006). Variables denoted Φ are the model-derived methane equilibrium flux and the isotopic signatures of the $^{13}CH_4$ and DCH_3 fluxes. Variables denoted τ depict the calculated chemical lifetimes of methane and its stable isotopes.

Budget parameter	ACT	PIH	LGM
$[CH_4]$ (ppb)	1675	724	362
$\delta^{13}C_{CH_4}$ (‰)	−47.5	−46.3	−42.8
δD_{CH_4} (‰)	−90	−100	−80
Φ_{CH_4} (Tg/yr)	523	242	137
$\delta^{13}C(\Phi_{CH_4})$ (‰)	−53	−51.5	−48.5
$\delta D(\Phi CH_4)$ (‰)	−300	−310	−296
[OH]moy (mol/cm^3)	12.2×10^5	13.8×10^5	15.7×10^5
τ_{CH_4} (yr)	8.17	7.70	6.89
$\tau_{^{13}CH_4}$ (yr)	8.22	7.74	6.93
τ_{DCH_3} (yr)	10.7	10.1	9.05

its chemical and photochemical reaction rates (Martinerie et al., 2009). The calculated methane lifetime for present-day conditions (Table 1) is consistent with the IPCC (2007) estimate of 8.7 ± 1.3 yrs. Boundary conditions from Martinerie et al. (1995) are used for the three simulated time periods. A major change in the past methane budget estimates since that study is the discovery of the large potential influence of volatile organic compounds (VOC) (Adams et al., 2001; Lathière et al., 2005) on the dominant methane sink: the hydroxyl radical (Kaplan et al., 2006; Valdes et al., 2005). Such influence may be tempered since Lelieveld et al. (2008) reported unexpectedly high OH concentrations above the Amazon forest, indicating that VOC oxidation efficiently recycles OH in low-NO_x environments. Moreover recent laboratory studies emphasize a CO_2 inhibition effect on isoprene emissions from plant leaves, which may have offset the strong temperature effect at least partially during glacial times (Arneth et al., 2007; Wilkinson et al., 2009). Published estimates of the change in OH mean concentration between the pre-industrial and last glacial periods are listed in the Supplementary material (Table S.1). Most models predict increased OH levels at Last Glacial Maximum. Our updated model produces a 14% increase (Table 1), which is somewhat lower than its previous version (20%, Martinerie et al., 1995) and the recent simulations which include a strong effect of VOCs (25–28%, Kaplan et al., 2006; Valdes et al., 2005). The updated model also leads to slightly higher OH at pre-industrial than present ($+10\%$), in contrast with previous results (-15%). These values are within the range of other model results (e.g., Harder et al., 2007; Thompson et al., 1993, and references therein). The above mentioned changes in OH remain much smaller than the changes in methane concentrations, implying that methane sources must play a major role on its concentration changes.

The fluxes of CH_4, $^{13}CH_4$ and DCH_3 required to produce steady state concentrations specified from ice core data (Table 1) were first calculated. They are expressed as net fluxes (emissions minus non modelled sinks) needed to compensate the modelled atmospheric sink (in the troposphere and the stratosphere). Note that the tropospheric Cl sink is incompletely modelled as the marine boundary layer Cl sink, driven by a complex heterogeneous source of chlorine (e.g., Allan et al., 2007) is not represented. We then added to these fluxes a pulse representing a clathrate emission. $\delta^{13}C_{CH_4}$ and δD_{CH_4} isotopic signatures for the clathrate emission were specified as -60‰ and -189‰ respectively (Fischer et al., 2008; Sowers, 2006, and references therein). The atmospheric fractionations by OH and Cl are taken into account for $^{13}CH_4$ and DCH_3 (Sander et al., 2006; Saueressig et al., 1995). The missing marine boundary layer chlorine in our model is unlikely to have a significant impact on our results as estimated changes in $\delta^{13}C_{CH_4}$ due to past changes in this minor methane sink (Levine et al., 2011b) are an order of magnitude lower than clathrate induced $\delta^{13}C_{CH_4}$ perturbations (see Section 3.2). Due to its lower reaction rate with OH, DCH_3 has a significantly longer lifetime than methane (Table 1). As will be seen in the following, this has important consequences on the δD signature of a clathrate degassing event.

2.2. The model of trace gas transport and trapping in firn

The above simulated atmospheric concentration trends are used as input to a model of trace gas transport in firn including progressive bubble enclosure (Witrant et al., 2011). This model showed very good performances in a recent inter-comparison study (Buizert et al., 2012). The two major processes leading to trace gas mixing in ice cores are gas transport in interstitial air of the firn (mainly controlled by firn diffusivity) and bubble close-off which occurs progressively within the deepest 5–10 m of the firn. The progressive air trapping in bubbles is simulated based on present-day open/closed porosity observations at three polar sites (Goujon et al., 2003). It depends at first order on the firn sinking speed and thus the accumulation rate. In this study, we apply the model to five well constrained drill sites (Martinerie et al., 2009; Witrant et al., 2011) covering a large range of temperatures and accumulation rates, and thus firn smoothing rates. Two of these sites are located in the Arctic (Devon Island and North GRIP), the three others are Antarctic sites (Berkner Island, Dronning Maud Land and Dome C). Firn diffusivity can be determined only for present-day climatic conditions. We thus use the same site characteristics (diffusivity, accumulation, temperature) for all simulated periods. This leads to likely under-estimated smoothing effects for LGM simulations, due primarily to the reduced snow accumulation rates at all sites. We thus further simulate the most arid and cold conditions at Dome C using reduced (LGM level) temperature and accumulation rate.

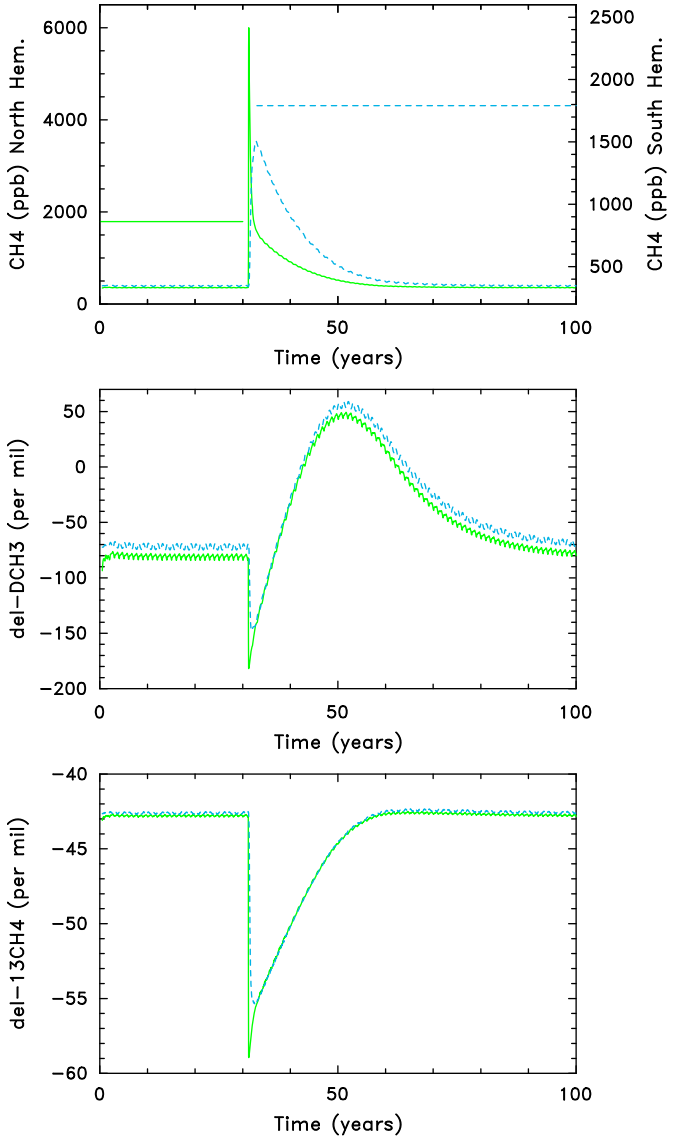

Fig. 1. Atmospheric trends in methane concentration (upper panel), δD_{CH_4} (middle panel) and $\delta^{13}C_{CH_4}$ (lower panel) at high latitudes. Continuous (green online) lines: 75°N, 3 km altitude and referring to the left scale, dashed (blue online) lines: 75°S, 3 km altitude and referring to the right scale for methane. The methane emission from clathrates (4000 Tg in one time step) occurs at 65°N in March, in LGM climatic conditions. Horizontal lines on upper panel show the theoretical global mean CH_4 concentration just after clathrate emission (1790 ppb).

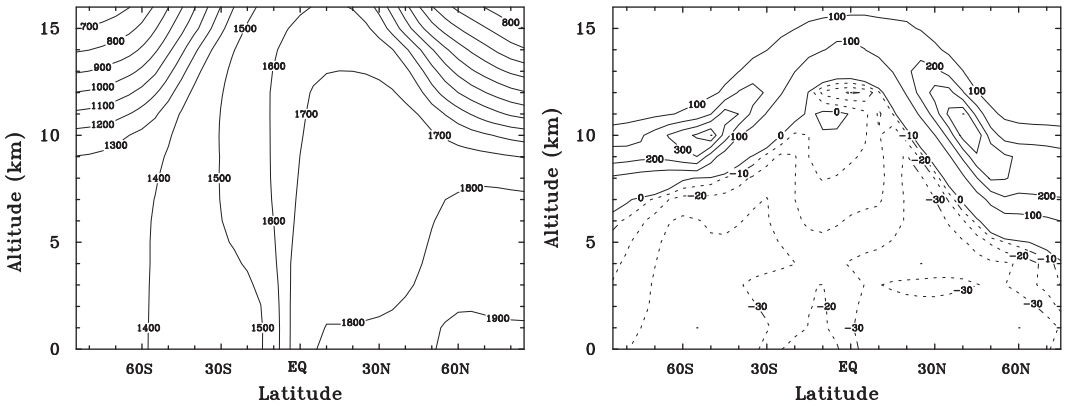

Fig. 2. Methane concentration (ppb, left panel) and OH difference from the equilibrium field (%, right panel), 1 yr after an emission from clathrates (4000 Tg CH_4 in one time step, at 65°N in March, in LGM climatic conditions).

Table 2
Atmospheric methane response to a clathrate emission. The first column indicates the simulated period. The second column shows the characteristics of the emission (latitude, intensity and duration). The peak amplitude shows the maximum CH_4 increase at 75° latitude in the hemisphere of the clathrate emission and $[CH_4]^{tropo}$ amplitude shows the increase in annual mean tropospheric methane (years start at pulse emission date). The numbers following ± signs indicate the amplitude variations due to the season of the clathrate emission. Peak width is the time required for global tropospheric methane to decay back to 10 ppb above its baseline level (10 ppb is the uncertainty on CH_4 measurements in ice cores, e.g. Spahni et al., 2003). The last column shows the maximum change in CH_4 mean annual lifetime.

Period	Conditions	Peak amplitude (ppb)	$[CH_4]^{tropo}$ amplitude (ppb)	Peak width (yrs)	τ_{max} amplitude (yrs)
ACT	65°N 4×10^3 Tg, pulse	13,042 ± 1100	1437 ± 130	60	1.1
ACT	15°S 4×10^3 Tg, pulse	3244 ± 155	1440 ± 10	62	1.3
ACT	65°N 4×10^3 Tg, 10 yr	2903	861	65	0.9
ACT	65°N 4×10^3 Tg, 50 yr	2062	306	92	0.5
ACT	65°N 1×10^3 Tg, pulse	4222	380	43	0.5
ACT	65°N 1×10^4 Tg, pulse	27,029	3846	75	2.7
PIH	65°N 4×10^3 Tg, pulse	12,106 ± 1120	1444 ± 130	55	2.7
PIH	15°S 4×10^3 Tg, pulse	2334 ± 155	1439 ± 9	57	2.3
PIH	65°N 4×10^3 Tg, 10 yr	1951	850	60	1.6
PIH	65°N 4×10^3 Tg, 50 yr	1095	284	87	0.7
PIH	65°N 1×10^3 Tg, pulse	3274	381	39	0.7
PIH	65°N 1×10^4 Tg, pulse	26,088	3874	70	5.0
LGM	65°N 4×10^3 Tg, pulse	9587 ± 2220	1415 ± 163	40	3.3
LGM	15°S 4×10^3 Tg, pulse	1981 ± 155	1427 ± 30	42	2.3
LGM	65°N 4×10^3 Tg, 10 yr	1436	767	45	1.3
LGM	65°N 4×10^3 Tg, 50 yr	646	230	79	0.6
LGM	65°N 1×10^3 Tg, pulse	1768	363	31	0.7
LGM	65°N 1×10^4 Tg, pulse	14,468	3713	52	5.3

3. Atmospheric impact of a large methane emission

In order to compare our results to those of Thorpe et al. (1996), we first used the same emission characteristics: a single time-step (15 days) emission of 4000 Tg CH_4 at 65°N in March, for the LGM period. We then tested the influences of the emission latitude (65°N or 15°S), season, intensity (1000–10,000 Tg CH_4) and duration (15 days to 50 yrs) for three climatic periods (present, PIH and LGM). Long simulations lasting for 142 to 202 yrs were performed to ensure complete stabilization of methane and its stable isotopic ratios before and after the pulse emission. In the firn model, equilibrium concentrations are used during longer time periods (see Section 4).

3.1. Atmospheric methane

As in Thorpe et al. (1996), very high concentrations, which can exceed 10,000 ppb, are obtained in the clathrate emission region one model time step after the pulse. The CH_4 spike is then more quickly diluted by atmospheric transport (in about a year, see Fig. 1) than destroyed (in about 7–8 yrs, see Table 1). The atmospheric mean concentration, assuming complete mixing and before a significant effect of the atmospheric sink, can be calculated from the emission flux and the atmospheric mass. A 4000 Tg CH_4 emission results in a 1433 ppb increase in CH_4 global mean concentration. Methane concentrations rapidly reach values within a few hundred ppb of this theoretical mean (Fig. 1). One year after the emission, the inter-polar concentration gradient is reduced to about 600 ppb (Fig. 2). This is lower than the equivalent gradient obtained by Thorpe et al. (1996): about 1500 ppb. However, our present-day modelled meridional transport has been validated with long-lived halocarbon transport (Martinerie et al., 2009). We obtain fairly similar values of the inter-polar concentration gradient for other simulated periods (about 800 ppb at present and PIH) despite the changes in OH and inter-hemispheric transport during the LGM. As a result of this fast atmospheric mixing and the smoothing effect of the firn, the latitude of the clathrate emission leaves no specific imprint in the ice core records of the methane mixing ratio (see Section 4.1). Thus in the following we will mostly discuss yearly averaged tropospheric mean results.

Table 2 displays the amplitudes and widths of methane perturbations for different simulations. The mean tropospheric amplitudes following a pulse emission are mostly independent

from the emission latitude and season and from climate conditions. These amplitudes largely exceed the recorded variations of methane concentrations in ice cores except for the 1000 Tg pulse emission and the 4000 Tg 50 yrs long emission.

The methane peak widths are primarily related to the OH levels and thus the methane lifetimes. Methane lifetime itself is affected by the amount of methane emitted, which reduces the global tropospheric OH. This effect can be evaluated using a simple global tropospheric mass balance calculation:

$$[CH_4](t+\Delta t) = [CH_4](t) + \Delta t\left(\Phi(t) - \frac{[CH_4](t)}{\tau(t)}\right) \quad (1)$$

where Φ represents the time-dependent methane emission and τ the equilibrium methane lifetime for the considered climatic period (see Table 1). The full set of results of such calculations for methane and its isotopes are provided in the Supplementary material (Tables S.2 and S.3). This effect leads to increased peak widths by 9–23 yrs in present and pre-industrial conditions, but we obtain only 3–9 yrs widening in LGM conditions. Test simulations showed that this non-linearity is independent from climatic parameters (temperature, winds, and water vapour) but disappears if NO_x emissions are slightly decreased to their PIH values in LGM simulations. Thus the complex coupling of the CH_4–HO_x–NO_x chemistry renders the effect of methane lifetime changes difficult to predict. Thorpe et al. (1996) obtain a somewhat longer return time to equilibrium than ours for LGM conditions (by about 10–20 yrs). The above non-linearity may contribute to this difference. Moreover their CH_4 equilibrium lifetimes are higher than ours, probably due to the re-evaluation of the CH_4+OH reaction rate since 1996. Overall, the effect of the methane sink perturbation is relatively small. The decrease in tropospheric OH is proportionally much smaller than the methane increase (Fig. 2). Using a three-dimensional chemistry transport model, Isaksen et al. (2011) performed several simulations involving strongly enhanced Arctic methane emissions. The hydrate release scenario used involves a stronger and longer emission than in our study: 50,000 Tg CH_4 in 1 yr, which induces a larger perturbation of the methane lifetime (increase by a factor 2.34). However, our results are roughly consistent with the relationship between methane burden and lifetime illustrated in Fig. 1 of Isaksen et al. (2011). We should note the enhanced OH concentrations in the upper troposphere after a clathrate emission (Fig. 2). This counter-intuitive feature is likely due to the enhanced water vapour production from methane oxidation, which favours the $O(^1D)$ reaction with H_2O, leading to two OH radicals. This also induces increased concentrations of tropospheric ozone (see Supplementary Fig. S.2). Similar behaviours of upper tropospheric OH and O_3 are obtained for the three simulated periods as well as by Isaksen et al. (2011) and Thorpe et al. (1996). Varying clathrate emission intensity has an almost linear effect on tropospheric mean CH_4 peak amplitude. This can be easily seen in Table 2 by comparing the effects of the 1000 and 10,000 Tg emissions.

The $\delta^{13}C$ records in foraminifera suggest that such events could have lasted for at least a decade (see Section 1). Methane emissions spread out (equally) over 10–50 yr were thus simulated. The tropospheric methane concentration then increases continuously until the end of the degassing. It results in lower amplitudes and longer durations of the CH_4 perturbations (see Table 2 and Supplementary Fig. S.1).

3.2. Atmospheric responses of methane stable isotopes

Immediately following a 4000 Tg pulse emission, $\delta^{13}C_{CH_4}$ and δD_{CH_4} tend toward the clathrate source signatures (−60‰ and −189‰ respectively, see Fig. 1) in the region of the emission. The minimum mean tropospheric values are higher ($\delta^{13}C_{CH_4} = -57.5$‰ and $\delta D_{CH_4} = -170$‰ in LGM simulations) and climate-dependent. Because methane from hydrates dilutes into a larger atmospheric reservoir, mean tropospheric signatures at pre-industrial ($\delta^{13}C_{CH_4} = -56.5$‰ and $\delta D_{CH_4} = -165$‰) and present-day ($\delta^{13}C_{CH_4} = -54.5$‰ and $\delta D_{CH_4} = -145$‰) are higher.

The return to equilibrium of isotopic signatures mainly results from two factors: fractionation by OH, which react faster with $^{12}CH_4$ than its heavier isotopologues and mixing with methane emitted by stationary sources. This induces different behaviours for $\delta^{13}C_{CH_4}$ and δD_{CH_4}. The clathrate methane source $\delta^{13}C$ signature is more negative than the mean signature of other methane sources (see Table 1), thus both source mixing and fractionation by OH lead to a reduction of $\delta^{13}C_{CH_4}$. This results in a $\delta^{13}C_{CH_4}$ return to equilibrium similar to the one of methane, albeit with opposite sign and slightly faster. In contrast, the clathrate methane source δD signature is less negative than the mean

Table 3
Mean tropospheric annual average response of $\delta^{13}C_{CH_4}$ and δD_{CH_4} to a clathrate emission. *A* stands for amplitude and *W* for width of the peaks. For δD_{CH_4}, A^- and W^- characterize the negative excursion from equilibrium and A^+ and W^+ characterize the positive excursion (see Fig. 1). Widths are defined as the time required to return to within 0.1 ‰ of equilibrium value for $\delta^{13}C_{CH_4}$ and 1 ‰ of equilibrium value for δD_{CH_4}.

Period	Conditions	A ($\delta^{13}C$) (‰)	W ($\delta^{13}C$) (yrs)	A^- (δD) (‰)	W^- (δD) (yrs)	A^+ (δD) (‰)	W^+ (δD) (yrs)
ACT	65°N 4×10^3 Tg, pulse	-5.7 ± 0.3	24	-44 ± 2	7	32 ± 3	77
ACT	15°S 4×10^3 Tg, pulse	-5.7 ± 0.1	24	-43 ± 0	7	36 ± 0	79
ACT	65°N 4×10^3 Tg, 10 yr	−3.5	29	−15	12	31	75
ACT	65°N 4×10^3 Tg, 50 yr	−1.1	61	−3.7	13	20	100
ACT	65°N 1×10^3 Tg, pulse	−2.3	19	−17	6	10	59
ACT	65°N 1×10^4 Tg, pulse	−8.6	27	−66	8	72	94
PIH	65°N 4×10^3 Tg, pulse	-9.0 ± 0.3	27	-57 ± 2	6	66 ± 5	81
PIH	15°S 4×10^3 Tg, pulse	-9.0 ± 0	27	-55 ± 0	6	73 ± 1	83
PIH	65°N 4×10^3 Tg, 10 yr	−6.1	32	−22	12	64	80
PIH	65°N 4×10^3 Tg, 50 yr	−2.3	64	−6.1	12	43	107
PIH	65°N 1×10^3 Tg, pulse	−4.7	22	−28	6	22	65
PIH	65°N 1×10^4 Tg, pulse	−11	32	−72	7	135	98
LGM	65°N 4×10^3 Tg, pulse	-14 ± 0.4	27	-83 ± 3	6	123 ± 10	75
LGM	15°S 4×10^3 Tg, pulse	-14 ± 0	27	-82 ± 1	7	135 ± 2	76
LGM	65°N 4×10^3 Tg, 10 yr	−10	32	−39	12	120	74
LGM	65°N 4×10^3 Tg, 50 yr	−4.6	68	−13	12	70	104
LGM	65°N 1×10^3 Tg, pulse	−8.6	25	−51	5	41	63
LGM	65°N 1×10^4 Tg, pulse	−16	33	−96	8	223	88

signature of other methane sources. Just after the pulse emission, an initial negative excursion of δD_{CH_4} reflecting the source signature is obtained. Then the following years show a dominant effect of OH fractionation, leading to a progressive increase in δD_{CH_4} and signatures exceeding the equilibrium δD_{CH_4} value (see Fig. 1). Afterwards, mixing with methane from other sources induce a decrease in δD_{CH_4} back to the equilibrium level.

Analogues of Eq. (1) can be used for $^{13}CH_4$ and DCH_3. They lead to global mean isotopic signatures overall consistent with model results (see Supplementary Table S.3), although less accurate for δD_{CH_4}. This is likely due to the strongly temperature-dependent DCH_3 fractionation by reaction with OH, which is not represented in simplified equations such as Eq. (1). These simple calculations allow to test the above interpretations and to investigate lifetime effects on $\delta^{13}C_{CH_4}$ and δD_{CH_4} peak widths. Using the overall methane lifetime instead of the individual lifetimes of the isotopes removes the effect of fractionation by OH. It leads to peak widths much closer to the CH_4 peak widths for both isotopes (see Supplementary Table S3). Thus the reduced length of the perturbation for $\delta^{13}C_{CH_4}$ and its increased length for δD_{CH_4} are mostly due to fractionation by OH.

As for methane, varying latitude and season of clathrate emission have a small influence on global mean $\delta^{13}C_{CH_4}$ and δD_{CH_4} peak amplitude and width. Increasing emission intensities lead to similarly shaped perturbations with increasing amplitude and width, but in contrast with methane, the increase is not linear. For instance the minimum $\delta^{13}C_{CH_4}$ and δD_{CH_4} values cannot be lower than the hydrate source signature, inducing a saturation effect on negative peak amplitudes. In addition, progressive clathrate emissions tend to delay and to reduce the atmospheric extrema while increasing the perturbation length.

3.3. Radiative forcing

The radiative code associated with our two-dimensional atmospheric model (Wang et al., 1991) is a band model dedicated to global climate simulations. In this section, we discuss its performance and evaluate both the direct and indirect radiative impacts of a methane emission from clathrates. It has been shown (IPCC, 2001) that band models overestimate the direct radiative forcing (RF) in comparison to line by line models. This effect was evaluated by comparing our present versus PIH RF with best estimates (IPCC, 2001, 2007). The results shown in Table 4 indicate a 30% overestimation by our model, which is consistent with the IPCC (2001) conclusion that band models generally overestimate direct RF by up to 50%. As a consequence, the simplified formula from Table 6.2 in IPCC (2001, p. 358), providing more consistent results with line by line models, is also used to estimate the direct RF of methane, and compared with our model results (Supplementary Table S.4).

For a 4000 Tg methane pulse, direct radiative forcing reaches a comparable amplitude (at present) or nearly twice the amplitude (for LGM) of the increase in methane RF between PIH and present (0.48 W/m^2, IPCC, 2007). Due to a saturation of some CH_4 absorption bands, the radiative forcing decreases with increasing background methane concentration. Our global mean RF for the LGM is comparable to the one calculated by Thorpe et al. (1996): 1 W/m^2, at a latitude distant from the clathrate emission (85°S).

Fig. 3 illustrates the total (direct+indirect) radiative impact of a methane release from clathrates calculated with our model. Here the indirect RF arising from chemical feedbacks linked to methane oxidation is taken into account. IPCC (2001) suggests that the total RF of methane is 20–75% larger than its direct RF. Consistently with this large interval, our result lead to a total RF about 50% higher than the direct RF. Although the total radiative forcing due to a 4000 Tg CH_4 burst can reach important values (up to 1.6 W/m^2), its short duration likely limits its impact due to the inertia of the climate system in terms of feedback processes. A 50 yr long emission increases the perturbation duration but strongly decreases its amplitude (Fig. 3). When integrated over time, cumulative perturbations for all simulations using the same climate conditions and a total emission of 4000 Tg CH_4 are somewhat similar (within $\pm$25%).

Table 4
Radiative forcing (RF) of background methane (W/m^2). IPCC direct forcings are calculated with the formula in Table 6.2 of IPCC (2001, p. 358), using the same concentrations as in our model (Table 1).

Reference	ACT-PIH		PIH-LGM	
	$RF^{direct}_{CH_4}$	$RF^{total}_{CH_4}$	$RF^{direct}_{CH_4}$	$RF^{total}_{CH_4}$
Martinerie et al. (1995)	0.62	0.93	0.38	0.50
This study	0.64	0.96	0.39	0.57
IPCC (2001, 2007)	0.44	0.58–0.84	0.26	–

4. Ice core record of a large methane emission

In this section, we aim at identifying ice core signal features that could best characterize methane hydrate destabilization events. The firn model was forced with concentrations computed by the atmospheric model at high latitudes. The atmospheric model simulations discussed above were performed over a sufficiently long time period (up to 200 yrs) to ensure a return to equilibrium of methane concentrations and isotopic ratios. The model of trace gas transport in firn was run for even longer time periods (up to 3800 yrs for Dome C) in order to reach full trapping in ice of the atmospheric perturbation. We used the equilibrium

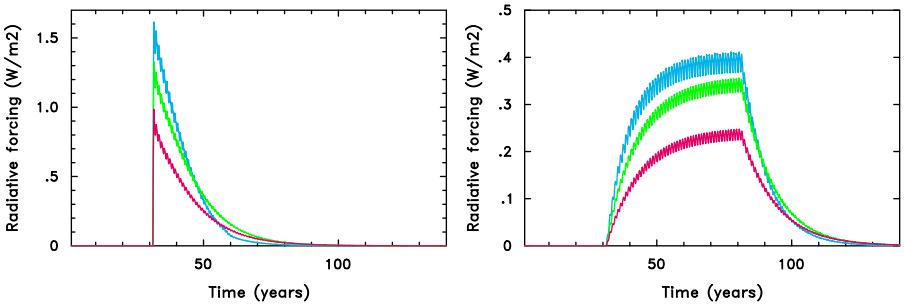

Fig. 3. Radiative forcing due to a methane emission from clathrates. Left panel: pulse emission, right panel: 50 yrs long emission (4000 Tg CH_4 at 65°N starting in March). Black(Red online): present conditions, dark grey(green online): PIH, light grey(blue online): LGM. Note the different vertical scales.

concentrations reached by the atmospheric model to extend the input concentration trend used by the firn model.

4.1. The methane signal in ice-cores

The diffusion into the firn of an atmospheric perturbation is driven by the concentration gradient between the upper and lower firn. Due to the depth dependence of firn porosity and tortuosity, this process is fast in the upper firn (a few days to a few months) and much slower in the bubble close-off zone (several decades). The diffusion process occurs in both directions. Thus when the atmospheric methane concentration decreases, CH_4 diffuses out of the firn. Our firn model is able to reproduce such a feature, as demonstrated in the case of CH_3CCl_3 changes over the last decades (Buizert et al., 2012; Witrant et al., 2011).

Because gas transport in firn and bubble closure smooth atmospheric trace gas variations, a strongly reduced methane peak height ($\sim$30% of the mean tropospheric amplitude at Devon Island and only $\sim$5% at Dome C, taking the two extremes among the studied sites) is obtained in ice for a pulse emission (Fig. 4, upper panel and Table 5). This peak amplitude is most sensitive to the simulated firn site (Fig. 5): an important increase is observed with the local snow accumulation rate (30 cm w eq yr^{-1} at Devon Island and 3.6 cm w eq yr^{-1} at Dome C). Using LGM temperature and accumulation conditions at Dome C (-64 °C,1.2 cm w eq yr^{-1}, Parrenin et al., 2007) further reduces the methane peak height to $\sim$1% of its atmospheric value. The full set of results for North GRIP (17 cm w eq yr^{-1}), Berkner Island (13 cm w eq yr^{-1}) and Dronning Maud Land (7 cm w eq yr^{-1}) is provided in Supplementary Table S.5 and shows intermediate values between Devon Island and Dome C. This is related to the bubble close-off duration: in our model, 90% of the firn bubbles close in the bottom 6–9 m of the firn. The time needed for a given firn layer to cross this bubble closure zone ranges from 20 yrs at Devon Island to 620 yrs at Dome C (with LGM accumulation). The reduction in peak amplitude is related to the short duration of the perturbation: the amplitude of a methane emission from hydrates during 50 yrs is fully preserved at Devon Island and reduced to 22% of the tropospheric mean concentration at Dome C (7% with reduced LGM accumulation). For this 50 yrs emission, the reduction of amplitude is 75% larger at Dome C than at North GRIP in interglacial conditions. This is qualitatively consistent with the 34–59% reduction between GRIP and Dome C observed by Spahni et al. (2003) for a longer (100–150 yrs) atmospheric perturbation. In contrast with peak amplitude, peak widths are markedly longer in ice than in the atmosphere (up to a factor of 6–8 for a 10,000 Tg pulse emission at Dome C). This widening increases the likeliness of detecting hydrate events through discrete sampling of ice cores.

Absolute peak amplitudes (in ppb) and widths (in metres of ice) in the ice vary little with the duration of the emission if the total emission is unchanged (Table 5). This integrator behaviour of the firn limits the possibility of reconstructing the characteristics of a short atmospheric perturbation from a single ice core. In contrast, pulse emissions of increasing intensity produce ice core signals of increasing intensity and width. The peak characteristics vary much less with the time period (present, PIH or LGM) or latitude of the emission at a given site than from site to site, in relation with their varying accumulation rates. As expected, the

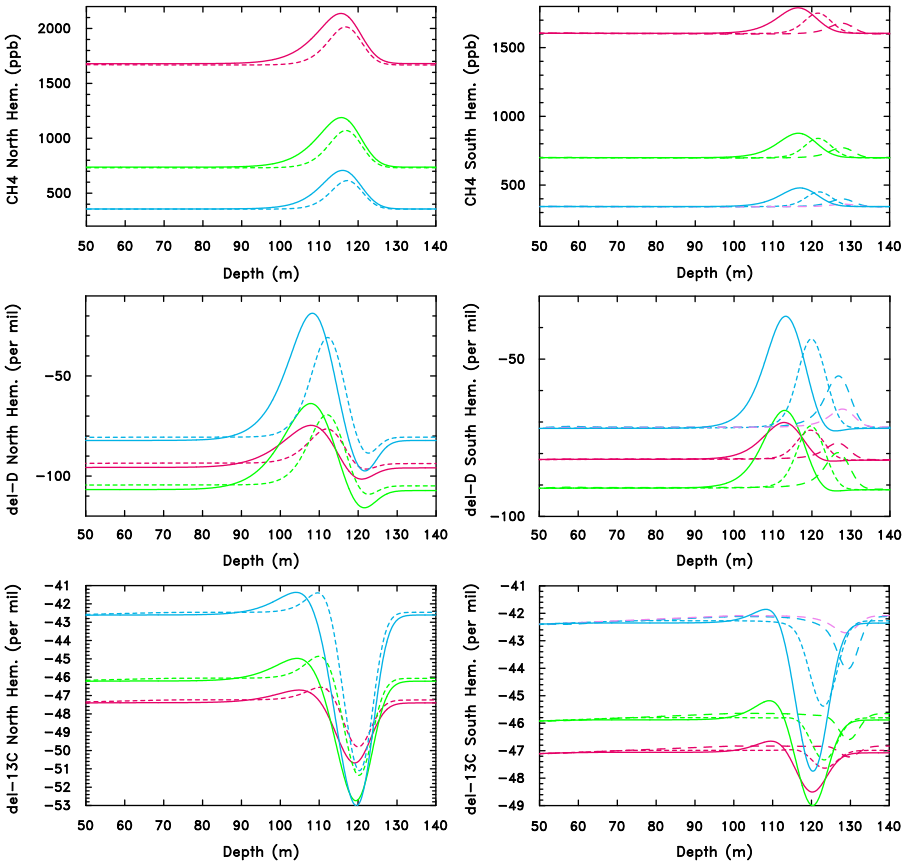

Fig. 4. CH_4, δD_{CH_4} and $\delta^{13}C_{CH_4}$ signals in ice cores following a 4000 Tg CH_4 pulse emission at 65°N in March. Black(Red online): present conditions, dark grey(green online): PIH, light grey(blue online): LGM. "Acc" values below are accumulation rates in cm w eq yr^{-1}. Left panel: Arctic sites (Devon Island: continuous lines, acc=30, North GRIP: short dashed lines, acc=17); right panel: Antarctic sites (Berkner Island: continuous lines, acc=13, Dronning Maud Land: short dashed lines, acc=7, Dome C: long dashed lines, acc=3.6. the lightest grey lines(purple lines online) show the Dome C results with reduced (LGM) temperature and accumulation rate (acc=1.2). Note the different vertical scales.

Table 5
Amplitudes and widths of methane, $\delta^{13}C_{CH_4}$ and δD_{CH_4} perturbations recorded in ice at Devon Island and Dome C. Notations and peak detection limits are the same as in Table 3. The values calculated for North GRIP, Berkner Island and Dronning Maud Land are provided in the Supplementary material, together with their conversion in fraction of the mean tropospheric peak amplitude and duration. LGM2 denotes Dome C simulations with reduced temperature and accumulation rate.

Period	Conditions	CH_4		$\delta^{13}C_{CH_4}$		$\delta^{13}C_{CH_4}$		δD_{CH_4}		δD_{CH_4}	
		A (ppb)	W (m)	A^+ (‰)	W^+ (m)	A^- (‰)	W^- (m)	A^+ (‰)	W^+ (m)	A^- (‰)	W^- (m)
Devon Island											
ACT	65°N 4×10^3 Tg, pulse	446 ± 43	36	0.7 ± 0.1	18	-3.3 ± 0.2	18	20 ± 2	30	-6 ± 1	11
ACT	15°S 4×10^3 Tg, pulse	397 ± 3	36	0.7 ± 0	18	-2.7 ± 0	17	23 ± 0	33	-2 ± 0	6
ACT	65°N 4×10^3 Tg, 10 yr	430	36	0.7	18	−3.1	18	19	30	−5.8	10
ACT	65°N 4×10^3 Tg, 50 yr	315	42	0.5	16	−1.8	25	15	35	−2.4	9
ACT	65°N 1×10^3 Tg, pulse	110	27	0.2	7	−0.9	14	6	23	−1.5	5
ACT	65°N 1×10^4 Tg, pulse	1207	43	1.6	24	−6.8	20	47	37	−13.4	12
PIH	65°N 4×10^3 Tg, pulse	440 ± 40	35	1.2 ± 0.1	21	-6.5 ± 0.4	20	40 ± 4	34	-10 ± 1	11
PIH	15°S 4×10^3 Tg, pulse	387 ± 3	35	1.2 ± 0	21	-5.5 ± 0	19	48 ± 1	37	-3 ± 0	6
PIH	65°N 4×10^3 Tg, 10 yr	421	35	1.2	21	−6.2	20	40	34	−9	11
PIH	65°N 4×10^3 Tg, 50 yr	300	41	0.9	19	−3.8	27	32	40	−3	10
PIH	65°N1 $\times10^3$ Tg, pulse	106	26	0.3	12	−2.0	17	13	28	−2	7
PIH	65°N 1×10^4 Tg, pulse	1228	42	2.6	26	−11.8	22	87	40	−19	13
LGM	65°N 4×10^3 Tg, pulse	360 ± 52	32	1.2 ± 0.2	19	-10.7 ± 0.9	22	59 ± 6	32	-19 ± 4	13
LGM	15°S 4×10^3 Tg, pulse	322 ± 8	31	1.3 ± 0	20	-9.6 ± 0.1	22	71 ± 2	36	-7 ± 1	9
LGM	65°N 4×10^3 Tg, 10 yr	335	31	1.2	19	−10.1	22	59	33	−16	12
LGM	65°N 4×10^3 Tg, 50 yr	241	38	0.9	18	−6.7	30	47	40	−7	12
LGM	65°N 1×10^3 Tg, pulse	81	23	0.4	12	−3.6	19	21	28	−4	8
LGM	65°N 1×10^4 Tg, pulse	1019	38	2.9	25	−17.1	24	119	38	−33	14
Dome C											
ACT	65°N 4×10^3 Tg, pulse	73 ± 8	14	0	0	-0.4 ± 0.1	7	5 ± 1	12	0	0
ACT	15°S 4×10^3 Tg, pulse	88 ± 2	15	0	0	-0.5 ± 0.1	8	5 ± 0	12	0	0
ACT	65°N 4×10^3 Tg, 10 yr	71	14	0	0	−0.4	7	5	12	0	0
ACT	65°N 4×10^3 Tg, 50 yr	69	14	0	0	−0.3	6	5	12	0	0
ACT	65°N 1×10^3 Tg, pulse	19	7	0	0	−0.1	0	1	5	0	0
ACT	65°N 1×10^4 Tg, pulse	213	19	0	0	−1.1	10	12	16	0	0
PIH	65°N 4×10^3 Tg, pulse	69 ± 8	14	0	0	-0.9 ± 0.1	10	11 ± 1	16	0	0
PIH	15°S 4×10^3 Tg, pulse	84 ± 2	15	0	0	-1.1 ± 0	11	11 ± 0	16	0	0
PIH	65°N 4×10^3 Tg, 10 yr	67	14	0	0	−0.8	10	11	16	0	0
PIH	65°N 4×10^3 Tg, 50 yr	63	13	0	0	−0.8	10	11	16	0	0
PIH	65°N 1×10^3 Tg, pulse	17	7	0	0	−0.2	5	3	9	0	0
PIH	65°N 1×10^4 Tg, pulse	213	19	0	0	−2.5	17	26	21	0	0
LGM	65°N 4×10^3 Tg, pulse	53 ± 8	12	0	0	-1.8 ± 0.2	16	16 ± 2	18	0	0
LGM	15°S 4×10^3 Tg, pulse	66 ± 2	13	0	0	-2.2 ± 0.1	18	16 ± 0	18	0	0
LGM	65°N 4×10^3 Tg, 10 yr	49	12	0	0	−1.7	16	16	18	0	0
LGM	65°N 4×10^3 Tg, 50 yr	50	12	0	0	−1.6	15	17	18	0	0
LGM	65°N 1×10^3 Tg, pulse	13	5	0	0	−0.5	9	5	12	0	0
LGM	65°N 1×10^4 Tg, pulse	174	18	0	0	−4.8	22	33	22	0	0
LGM2	65°N 4×10^3 Tg, pulse	17 ± 2	6	0	0	-0.6 ± 0.1	12	5 ± 1	13	0	0
LGM2	15°S 4×10^3 Tg, pulse	21 ± 1	8	0	0	-0.7 ± 0	13	6 ± 0	13	0	0
LGM2	65°N 4×10^3 Tg, 10 yr	16	6	0	0	−0.5	11	6	13	0	0
LGM2	65°N 4×10^3 Tg, 50 yr	16	6	0	0	−0.5	11	6	13	0	0
LGM2	65°N 1×10^3 Tg, pulse	6	0	0	0	−0.1	0	2	6	0	0
LGM2	65°N 1×10^4 Tg, pulse	57	13	0	0	−1.8	18	13	18	0	0

sites with largest accumulation rates provide less distorted records of a clathrate pulse. Nevertheless, in the least favourable case of Dome C, the imprint of a 4000 Tg pulse emission still leads to a 15–22 ppbv anomaly in CH_4 under LGM conditions, i.e. well above the analytical uncertainties. The Dome C ice layer thinning for the LGM period being $\sim$0.8, the anomaly would be recorded over about 9 m of core. It could thus be detected with the current resolution of the Dome C CH_4 record (Loulergue et al., 2008).

4.2. Methane isotopes recorded in ice-cores

Atmospheric trends in the isotopic composition of trace gases are modified in firn, as two main processes lead to isotopic fractionation (see e.g., Trudinger et al., 1997, the influence of thermal fractionation is neglected here). The first one is gravitational settling, which slightly enriches the deep firn with the heavier isotopologue. The second one is due to small differences between molecular diffusion coefficients of the isotopes, the heavier isotopologue diffuses slower. This diffusional fractionation largely dominates in a context of rapidly varying concentrations. Due to this process, a rapid increase in atmospheric methane without changing isotopic ratios results in negative $\delta^{13}C_{CH_4}$ and δD_{CH_4} anomalies in the firn. Similarly, a rapid CH_4 decrease implies a slower diffusion out of the firn of $^{13}C_{CH_4}$ than $^{12}C_{CH_4}$ and produces a positive $\delta^{13}C_{CH_4}$ (or δD_{CH_4}) anomaly. In order to quantify these effects, test simulations were performed with the same diffusion coefficient for CH_4, $^{13}C_{CH_4}$ and D_{CH_4} (see Supplementary Table S.7).

In the context of a massive methane emission from hydrates, diffusional fractionation results in "lying S" shaped signals in ice for both $\delta^{13}C_{CH_4}$ and δD_{CH_4} at high accumulation rate sites (Fig. 4), whereas atmospheric CH_4 and $\delta^{13}C_{CH_4}$ show a single peak. At low

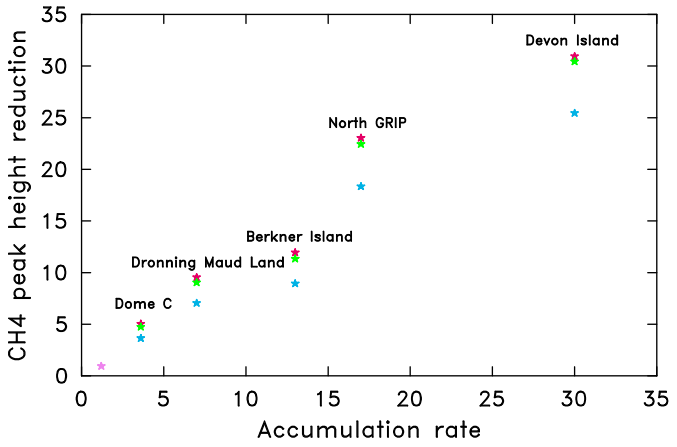

Fig. 5. Relative amplitude (%) of the methane peak in ice with respect to the mean tropospheric signal plotted versus snow accumulation rate (cm w. eq. yr^{-1}) at the modelled polar sites. Results are shown for a 4000 Tg CH_4 pulse emission at 65°N in March. Black(Red online): present conditions, dark grey(green online): PIH, light grey(blue online): LGM, lightest grey(purple online): LGM with reduced temperature and accumulation rate (acc=1.2).

accumulation rate sites, the longer duration of bubble closure increases smoothing time and lead to single peak shaped isotopic anomalies in ice. Surprisingly, the initially negative δD_{CH_4} anomaly disappears, i.e. the depletion of atmospheric δD_{CH_4} reflecting the hydrate source effect is lost. The later positive δD_{CH_4} atmospheric anomaly due to OH fractionation dominates in ice records. This feature persists in simulations using the same diffusion coefficient for all CH_4 isotopologues (see Supplementary Table S.7). Thus it results from the longer smoothing during gas trapping rather than from isotopic fractionation in firn.

Although complex, the behaviour of δD_{CH_4} in ice at high accumulation rate sites preserves an information on the latitude of the emission that is not observable in the methane record (Table 5): the amplitude and width of the negative δD_{CH_4} excursion is much larger (by a factor of $\sim 2-4$) for a high latitude emission close to the ice drilling site than for a distant emission (15°S). This provides a new indicator of the hemisphere where the methane burst took place: comparative measurements of the relative heights of the negative and positive anomaly (A^-/A^+) at Arctic and Antarctic sites of equivalent accumulation rates.

4.3. *Characterizing a methane emission from clathrates in ice-core records*

Greenland ice core records show several methane variations of about 100–200 ppb spanning about 100–200 yrs (e.g., Flückiger et al., 2004; Severinghaus et al., 1998). Due to the smoothing effect of firn and bubble closure, a hypothetical short term massive emission from marine hydrates, such as the 4000 Tg CH_4 pulse simulated here, would loose about 70% of its atmospheric amplitude in high accumulation rate records, and up to $\sim 99\%$ in low accumulation rate records of the Antarctic plateau and LGM conditions. However, the perturbation would span a relatively large depth range (~ 9 m) under low accumulation rate, with an amplitude still well above analytical uncertainties (see Section 4.1). Longer duration clathrate bursts would leave a wider imprint in ice cores, but would then not be distinguishable (through a characteristic transient signature) from other possible methane sources varying on long time scales (wetlands, biomass burning, atmospheric oxidation, etc.).

The methane isotope signatures are affected by dilution into a variable atmospheric burden of methane, fractionation (due to atmospheric OH and molecular diffusion in firn) and gas trapping at different time scales. Thus the amplitude and sign of the perturbations in $\delta^{13}C_{CH_4}$ and δD_{CH_4} in ice cores due to a clathrate destabilization event is not straightforward. The few available methane isotopic records in ice cores show variations in the ranges -42.5 to -49.5‰ for $\delta^{13}C_{CH_4}$ (Ferretti et al., 2005; Fischer et al., 2008; Mischler et al., 2009; Schaefer et al., 2006) and -70 to -115‰ for δD_{CH_4} (Bock et al., 2010; Mischler et al., 2009; Sowers, 2006). Our calculated isotopic signatures associated with clathrate degassing events cover a similar range at relatively low accumulation rate sites. Due to the smoothing effect of firn, fractional diffusion and bubble closure, the initial δD_{CH_4} clathrate source signature simulated in the atmosphere is smoothed out and even vanishes at low accumulation rate sites. Instead, transient isotopic signatures reflecting fractionation by atmospheric OH and mixing with atmospheric methane from non-hydrate sources are obtained.

An interesting feature in our results is that peak values of the methane, $\delta^{13}C_{CH_4}$ and δD_{CH_4} perturbations are recorded at different depths. This originates from the different duration and shape (for δD_{CH_4}) of their atmospheric perturbations (see Section 3.2). The minimum value in $\delta^{13}C_{CH_4}$ occurs at a deeper level than the methane peak, whereas the maximum δD_{CH_4} value occurs at shallower depth (Fig. 4). The width of these shift (1–10 m, not taking into account ice layers thinning with depth) is mainly accumulation rate dependent, but a slight shift is preserved even at Dome C (see Supplementary Fig. S.4 for a 50 yrs long emission). Expressed in terms of ice age differences, these shifts show a somewhat complex behaviour. Fractional diffusion in firn favours an early negative peak of $\delta^{13}C_{CH_4}$ in ice, especially at low accumulation rate sites, resulting in a 8–60 yrs time advance in our simulations, whereas no such shift is simulated in the atmosphere (within a year) for pulse emissions. The positive anomaly in δD_{CH_4} in ice shows a less variable time delay (15–38 yrs) with respect to the methane peak, whereas variable time delays are simulated in the atmosphere (8–27 yrs). Thus the complex interplay between fractionation in firn and the smoothing of the "lying S" shape atmospheric signature in δD_{CH_4} results in a somewhat steady age shift between CH_4 and δD_{CH_4} peaks in ice.

A target investigation of ice core records of clathrate degassing should rely on high resolution measurements of δD_{CH_4} at high accumulation rate sites in both hemispheres. A "lying S" shaped δD_{CH_4}-time trend should be observed, with an initially negative anomaly (resulting from a partially smoothed source effect), followed by a positive anomaly (arising from OH fractionation and mixing with non clathrate sources). The amplitude ratio between the positive and negative δD_{CH_4} swings in both hemisphere could constrain the latitude of clathrate emission (see Section 4.2).

The amplitudes of the δD_{CH_4} and $\delta^{13}C_{CH_4}$ anomalies undergo strong variations with the snow accumulation rate and climate conditions. However, the amplitude ratio: $A^+(\delta D_{CH_4})/A^-(\delta^{13}C_{CH_4})$ shows a more stable behaviour and remains in the range 5–16 for all simulated conditions. This range is close to the one calculated in the atmosphere: 4–19.

In summary, ice core records of a short time scale and massive methane emission from clathrates are characterized by accumulation rate dependent peak heights and depth shifts between the resulting perturbations in CH_4, δD_{CH_4} and $\delta^{13}C_{CH_4}$. The hydrate source can be identified by a "lying S" shaped signature of δD_{CH_4} at high accumulation rate sites and a peak amplitude ratio $A^+(\delta D_{CH_4})/A^-(\delta^{13}C_{CH_4})$ in the range ~ 5 to ~ 16.

5. Conclusions

This study thoroughly investigated the impact of massive methane emissions from hydrates and their imprints in ice cores,

through the combined use of an atmospheric chemistry model and a model of trace gas transport and bubble enclosure in firn. A 4000 Tg CH_4 emission results in a near doubling of the present-day atmospheric burden in methane. The associated radiative forcing is comparable to the one induced by the increase of methane between pre-industrial times and present. However, the short duration (decades) of the simulated clathrate-induced atmospheric perturbations likely limits their climatic impacts. Consistently with Isaksen et al. (2011), a limited decrease in the main methane sink: OH radicals is obtained for CH_4 emissions in the range 1000–10,000 Tg CH_4. As a consequence, varying the emission intensity has an almost linear effect on the atmospheric methane peak amplitude. In contrast, $\delta^{13}C_{CH_4}$ and δD_{CH_4} atmospheric trends show a non-linear and climate-dependent behaviour due to the combined effects of fractionation by OH and dilution of clathrate methane into atmospheric methane from other sources.

The amplitudes of most simulated atmospheric perturbations in methane and its stable isotopes largely exceed their recorded values in ice cores. The short durations of these perturbations, which occur at a similar or shorter time scale as bubble closure in ice, lead to a strong smoothing of their ice core imprints. The ice-core smoothing rates are highly dependent on the snow accumulation rate at the studied sites and overall consistent with the smoothing calculated by Spahni et al. (2003). Due to this smoothing effect, the simulated clathrate degassing events lead to perturbations in ice cores that do not always exceed the amplitude of some rapid events observed in existing records.

The best way to identify a clathrate degassing event in ice cores is to perform high resolution measurements of δD_{CH_4}. A "lying S" shaped signature in δD_{CH_4} at high accumulation rate sites should appear, reflecting the combined effects of the source signature and OH fractionation. Comparing Arctic and Antarctic records of δD_{CH_4} under similar accumulation rate conditions provides a way to constrain the latitude of a clathrate degassing event. Furthermore, the amplitude ratio in the maximum perturbations of $\delta^{13}C_{CH_4}$ and δD_{CH_4} is fairly well preserved in ice cores at all sites.

Acknowledgements

We are grateful to three anonymous referees for their constructive comments, which significantly improved our manuscript. This work was supported by the LGGE core budget, the CNRS/INSU LEFE program and the French ANR NEEM (ANR-07-VULN-09-001). It was also supported by the Past4Future project of the European Commission's 7th Framework Programme under Grant agreement no 243908 and is Past4Future contribution number 17. Firn air pumping operations at the five modelled polar sites were performed in the frame of EC programmes EUK2-CT2001-00116 (CRYOSTAT) and ENV4-CT97-0406 (FIRETRACC).

Appendix A. Supplementary data

Supplementary data associated with this article can be found in the online version at http://dx.doi.org.10.1016/j.epsl.2012.06.052.

References

Adams, J.M., Constable, J.V.H., Guenther, A.B., Zimmerman, P., 2001. An estimate of natural volatile organic compound emissions from vegetation since the last glacial maximum. Chemosphere—Global Change Sci. 3, 73–91.

Allan, W., Struthers, H., Lowe, D.C., 2007. Methane carbon isotope effects caused by atomic chlorine in the marine boundary layer: global model results compared with Southern Hemisphere measurements. J. Geophys. Res. 112, D04306.

Archer, D., 2007. Methane hydrate stability and anthropogenic climate change. Biogeosciences 4, 521–544.

Archer, D., Buffett, B., Brovkin, V., 2009. Ocean methane hydrates as a slow tipping point in the global carbon cycle. Proc. Natl Acad. Sci. U.S.A. 106, 20596–20601.

Arneth, A., Niinemets, Ü., Pressley, S., Bäck, J., Hari, P., Karl, T., Noe, S., Prentice, I.C., Serça, D., Hickler, T., Wolf, A., Smith, B., 2007. Process-based estimates of terrestrial ecosystem isoprene emissions: incorporating the effects of a direct CO_2-isoprene interaction. Atmos. Chem. Phys. 7, 31–53.

Bock, M., Schmitt, J., Möller, L., Spahni, R., Blunier, T., Fischer, H., 2010. Hydrogen isotopes preclude marine hydrate CH_4 emissions at the onset of Dansgaard–Oeschger events. Science 328, 1686–1689.

Brasseur, G., Hitchman, M.H., Walters, S., Dymek, M., Falise, E., Pirre, M., 1990. An interactive chemical dynamical radiative two-dimensional model of the middle atmosphere. J. Geophys. Res. 95, 5639–5655.

Brook, E.J., Harder, S., Severinghaus, J., Steig, E.J., Sucher, C.M., 2000. On the origin and timing of rapid changes in atmospheric methane during the last glacial period. Global Biogeochem. Cycles 14, 559–572.

Brook, E.J., White, J.W.C., Schilla, A.S.M., Bender, M.L., Barnett, B., Severinghaus, J.P., Taylor, K.C., Alley, R.B., Steig, E.J., 2005. Timing of millennial-scale climate change at Siple Dome, West Antarctica, during the last glacial period. Quat. Sci. Rev. 24, 1333–1343.

Buffett, B., Archer, D., 2004. Global inventory of methane clathrate: sensitivity to changes in the deep ocean. Earth Planet. Sci. Lett. 227, 185–199.

Buizert, C., Martinerie, P., Petrenko, V.V., Severinghaus, J.P., Trudinger, C.M., Witrant, E., Rosen, J.L., Orsi, A.J., Rubino, M., Etheridge, D.M., Steele, L.P., Hogan, C., Laube, J.C., Sturges, W.T., Levchenko, V.A., Smith, A.M., Levin, I., Conway, T.J., Dlugokencky, E.J., Lang, P.M., Kawamura, K., Jenk, T.M., White, J.W.C., Sowers, T., Schwander, J., Blunier, T., 2012. Gas transport in firn: multiple-tracer characterisation and model intercomparison for NEEM, Northern Greenland. Atmos. Chem. Phys. 12, 4259–4277.

Bünz, S., Mienert, J., Berndt, C., 2003. Geological controls on the Storegga gas-hydrate system of the mid-Norwegian continental margin. Earth Planet. Sci. Lett. 209, 291–307.

Cannariato, K.G., Stott, L.D., 2004. Evidence against clathrate-derived methane release to Santa Barbara basin surface waters? Geochem. Geophys. Geosyst. 5, Q05007.

de Garidel-Thoron, T., Beaufort, L., Bassinot, F., Henry, P., 2004. Evidence for large methane releases to the atmosphere from deep-sea gas-hydrate dissociation during the last glacial episode. Proc. Natl. Acad. Sci. U.S.A. 101, 9187–9192.

Dlugokencky, E.J., Nisbet, E.G., Fischer, R., Lowry, D., 2011. Global atmospheric methane: budget, changes and dangers. Philos. Trans. R. Soc. A 369, 2058–2072.

Etheridge, D.M., Steele, L.P., Francey, R.J., Langenfelds, R.L., 1998. Atmospheric methane between 1000 A.D. and present: evidence of anthropogenic emissions and climatic variability. J. Geophys. Res. 103, 15979–15993.

Etiope, G., Klusman, R.W., 2010. Microseepage in drylands: Flux and implications in the global atmospheric source/sink budget of methane. Global Planet. Change 72, 265–274.

Ferretti, D.F., Miller, J.B., White, J.W.C., Etheridge, D.M., Lassey, K.R., Lowe, D.C., Meure, C.M.M., Dreier, M.F., Trudinger, C.M., van Ommen, T.D., Langenfelds, R.L., 2005. Unexpected changes to the global methane budget over the past 2000 years. Science 309, 1714–1717.

Fischer, H., Behrens, M., Bock, M., Richter, U., Schmitt, J., Loulergue, L., Chappellaz, J., Spahni, R., Blunier, T., Leuenberger, M., Stocker, T.F., 2008. Changing boreal methane sources and constant biomass burning during the last termination. Nature 452, 864–867.

Flückiger, J., Blunier, T., Stauffer, B., Chappellaz, J., Spahni, R., Kawamura, K., Schwander, J., Stocker, T.F., Dahl-Jensen, D., 2004. N_2O and CH_4 variations during the last glacial epoch: insight into global processes. Global Biogeochem. Cycles 18, GB1020.

Flückiger, J., Dällenbach, A., Blunier, T., Stauffer, B., Stocker, T.F., Raynaud, D., Barnola, J.-M., 1999. Variations in atmospheric N_2O concentration during abrupt climatic changes. Science 285, 227–230.

Flückiger, J., Monnin, E., Stauffer, B., Schwander, J., Stocker, T.F., Chappellaz, J., Raynaud, D., Barnola, J.-M., 2002. High-resolution Holocene N_2O ice core record and its relationship with CH_4 and CO_2. Global Biogeochem. Cycles 16, 1010.

Goujon, C., Barnola, J.-M., Ritz, C., 2003. Modeling the densification of firn including heat diffusion: application to close-off characteristics and gas isotopic fractionation for Antarctica and Greenland sites. J. Geophys. Res. 108 (D24), 4792.

Harder, S.L., Shindell, D.T., Schmidt, G.A., Brook, E.J., 2007. A global climate model study of CH_4 emissions during the Holocene and glacial–interglacial transitions constrained by ice core data. Global Biogeochem. Cycles 21, GB1011.

IPCC, 2001. Climate Change 2001: The Scientific Basis, Contribution of Working Group I to the Third Assessment Report. Cambridge University Press, Cambridge, UK and New York, USA.

IPCC, 2007. Climate Change 2007: The Physical Science Basis. Contribution of Working Group I to the Fourth Assessment Report of the Intergovernmental Panel on Climate Change. Cambridge University Press, United Kingdom and New York, NY, USA. 〈http://www.ipcc.ch/ipccreports/assessments-reports.htm〉.

Isaksen, I.S.A., Gauss, M., Myhre, G., Walter Anthony, K.M., Ruppel, C., 2011. Strong atmospheric chemistry feedback to climate warming from Arctic methane emissions. Global Biogeochem. Cycles, GB2002.

Kaplan, J.O., Folberth, G., Hauglustaine, D.A., 2006. Role of methane and biogenic volatile organic compound sources in late glacial and Holocene fluctuations of atmospheric methane concentrations. Global Biogeochem. Cycles 20, GB2016.

Kennett, J.P., Cannariato, K.G., Hendy, I.L., Behl, R.J., 2000. Carbon isotopic evidence for methane hydrate instability during quaternary interstadials. Science 288, 128–133.

Kessler, J.D., Valentine, D.L., Redmond, M.C., Du, M., Chan, E.W., Mendes, S.D., Quiroz, E.W., Villanueva, C.J., Shusta, S.S., Werra, L.M., Yvon-Lewis, S.A., Weber, T.C., 2011. A persistent oxygen anomaly reveals the fate of spilled methane in the deep Gulf of Mexico. Science 331, 312–315.

Lambert, G., Chappellaz, J., Foucher, J.-P., Ramstein, G., 2006. Le méthane et le destin de la Terre—Les hydrates de méthane: rêve ou cauchemar? EDP Sciences, Les Ulis, France.

Lathière, J., Hauglustaine, D.A., De Noblet-Ducoudré, N., Krinner, G., Folberth, G.A., 2005. Past and future changes in biogenic volatile organic compound emissions simulated with a global dynamic vegetation model. Geophys. Res. Lett. 32, L20818.

Lelieveld, J., Butler, T.M., Crowley, J.N., Dillon, T.J., Fischer, H., Ganzeveld, L., Harder, H., Lawrence, M.G., Martinez, M., Taraborrelli, D., Williams, J., 2008. Atmospheric oxidation capacity sustained by a tropical forest. Nature 452, 737–740.

Levine, J.G., Wolff, E.W., Jones, A.E., Hutterli, M.A., Wild, O., Carver, G.D., Pyle, J.A., 2011a. In search of an ice core signal to differentiate between source-driven and sink-driven changes in atmospheric methane. J. Geophys. Res. 116, D05305.

Levine, J.G., Wolff, E.W., Jones, A.E., Sime, L.C., 2011b. The role of atomic chlorine in glacial–interglacial changes in the carbon-13 content of atmospheric methane. Geophys. Res. Lett. 38, L04801.

Loulergue, L., Schilt, A., Spahni, R., Masson-Delmotte, V., Blunier, T., Lemieux, B., Barnola, J.-M., Raynaud, D., Stocker, T.F., Chappellaz, J., 2008. Orbital and millennial-scale features of atmospheric CH_4 over the past 800,000 years. Nature 453, 383–386.

Martinerie, P., Brasseur, G.P., Granier, C., 1995. The chemical composition of ancient atmospheres: a model study constrained by ice core data. J. Geophys. Res. 100, 14291–14304.

Martinerie, P., Nourtier-Mazauric, E., Barnola, J.-M., Sturges, W.T., Worton, D.R., Atlas, E., Gohar, L.K., Shine, K.P., Brasseur, G.P., 2009. Long-lived halocarbon trends and budgets from atmospheric chemistry modelling constrained with measurements in polar firn. Atmos. Chem. Phys. 9, 3911–3934.

Maslin, M., Owen, M., Betts, R., Day, S., Dunkey Jones, T., Ridgwell, A., 2010. Gas hydrates: past and future geohazard? Philos. Trans. R. Soc. A 368, 2369–2393.

Maslin, M., Owen, M., Day, S., Long, D., 2004. Linking continental-slope failures and climate change: testing the clathrate gun hypothesis. Geology 32, 53–56.

Maslin, M., Vilela, C., Mikkelsen, N., Grootes, P., 2005. Causes of catastrophic sediment failures of the Amazon Fan. Quat. Sci. Rev. 24, 2180–2193.

Milkov, A.V., 2004. Global estimates of hydrate-bound gas in marine sediments: how much is really out there? Earth Sci. Rev. 66, 183–197.

Milkov, A.V., 2005. Molecular and stable isotope compositions of natural gas hydrates: a revised global dataset and basic interpretations in the context of geological settings. Org. Geochem. 36, 681–702.

Mischler, J.A., Sowers, T.A., Alley, R.B., Battle, M., McConnell, J.R., Mitchell, L., Popp, T., Sofen, E., Spencer, M.K., 2009. Carbon and hydrogen isotopic composition of methane over the last 1000 years. Global Biogeochem. Cycles 23, GB4024.

Nisbet, E.G., 1990. The end of the ice age. Can. J. Earth Sci. 27, 148–157.

Nisbet, E.G., 2002. Have sudden large releases of methane from geological reservoirs occurred since the last glacial maximum, and could such releases occur again? Philos. Trans. R. Soc. A 360, 581–607.

O'Hara, K.D., 2008. A model for late quaternary methane ice core signals: wetlands versus a shallow marine source. Geophys. Res. Lett. 35, L02712.

Parrenin, F., Dreyfus, G., Durand, G., Fujita, S., Gagliardini, O., Gillet, F., Jouzel, J., Kawamura, K., Lhomme, N., Masson-Delmotte, V., Ritz, C., Schwander, J., Shoji, H., Uemura, R., Watanabe, O., Yoshida, N., 2007. 1-D-ice flow modelling at EPICA Dome C and Dome Fuji, East Antarctica. Clim. Past 3, 243–259. 〈http://www.clim-past.net/3/243/2007/〉.

Paull, C.K., Ussler III, W., Holbrook, W.S., 2007. Assessing methane release from the colossal Storegga submarine landslide. Geophys. Res. Lett. 34, L04601.

Petrenko, V.V., Smith, A.M., Brook, E.J., Lowe, D., Riedel, K., Brailsford, G., Hua, Q., Schaefer, H., Reeh, N., Weiss, R.F., Etheridge, D., Severinghaus, J.P., 2009. $^{14}CH_4$ measurements in Greenland ice: investigating last glacial termination CH_4 sources. Science 324, 506–508.

Prokopenko, A.A., Williams, D.F., 2004. Deglacial methane emission signals in the carbon isotopic record of lake Baikal. Earth Planet. Sci. Lett. 218, 135–147.

Sander, S.P., Friedl, R.R., Golden, D.M., Kurylo, M.J., Moortgat, G.K., Keller-Rudek, H., Wine, P.H., Ravishankara, A.R., Kolb, C.E., Molina, M.J., Finlayson-Pitts, B.J., Huie, R.E., Orkin, V.L., 2006. Chemical Kinetics and Photochemical Data for Use in Atmospheric Studies, Evaluation Number 15. JPL Publication, vol. 06-2. Jet Propulsion Laboratory, Pasadena, California, USA. URL 〈http://jpldataeval.jpl.nasa.gov〉.

Saueressig, G., Bergamaschi, P., Crowley, J.N., Fischer, H., Harris, G.W., 1995. Carbon kinetic isotope effect in the reaction of CH_4 with Cl atoms. Geophys. Res. Lett. 22, 1225–1228.

Schaefer, H., Whiticar, M.J., Brook, E.J., Petrenko, V.V., Ferretti, D.F., Severinghaus, J.P., 2006. Ice record of $\delta^{13}C$ for atmospheric CH_4 across the Younger Dryas–Preboreal transition. Science 313, 1109–1112.

Schüpbach, S., Federer, U., Kaufmann, P.R., Hutterli, M.A., Buiron, D., Blunier, T., Fischer, H., Stocker, T.F., 2009. A new method for high-resolution methane measurements on polar ice cores using continuous flow analysis. Environ. Sci. Technol. 43, 5371–5376.

Severinghaus, J.P., Sowers, T., Brook, E.J., Alley, R.B., Bender, M.L., 1998. Timing of abrupt climate change at the end of the Younger Dryas interval from thermally fractionated gases in polar ice. Nature 391, 141–146.

Smith, L.M., Sachs, J.P., Jennings, A.E., Anderson, D.M., de Vernal, A., 2001. Light $\delta^{13}C$ events during deglaciation of the East Greenland continental shelf attributed to methane release from gas hydrates. Geophys. Res. Lett. 28, 2217–2220.

Sowers, T., 2006. Late quaternary atmospheric CH_4 isotope record suggests marine clathrates are stable. Science 311, 838–840.

Sowers, T., Alley, R.B., Jubenville, J., 2003. Ice core records of atmospheric N_2O covering the last 106,000 years. Science 301, 945–948.

Spahni, R., Chappellaz, J., Stocker, T.F., Loulergue, L., Hausammann, G., Kawamura, K., Flückiger, J., Schwander, J., Raynaud, D., Masson-Delmotte, V., Jouzel, J., 2005. Atmospheric methane and nitrous oxide of the late Pleistocene from Antarctic ice cores. Science 310, 1317–1321.

Spahni, R., Schwander, J., Flückiger, J., Stauffer, B., Chappellaz, J., Raynaud, D., 2003. The attenuation of fast atmospheric CH_4 variations recorded in polar ice cores. Geophys. Res. Lett. 30, 1571.

Stott, L.D., Bunn, T., Prokopenko, M., Mahn, C., Gieskes, J., Bernhard, J.M., 2002. Does the oxidation of methane leave an isotopic fingerprint in the geologic record? Geochem. Geophys. Geosyst. 3, 1012.

Thompson, A.M., Chappellaz, J.A., Fung, I.Y., Kucsera, T.L., 1993. The atmospheric CH_4 increase since the last glacial maximum (2). Interactions with oxidants. Tellus 45B, 242–257.

Thorpe, R.B., Law, K.S., Bekki, S., Pyle, J.A., Nisbet, E.G., 1996. Is methane-driven deglaciation consistent with the ice core record? J. Geophys. Res. 101, 28627–28635.

Torres, M.E., Mix, A.C., Kinports, K., Haley, B., Klinkhammer, G.P., McManus, J., deAngelis, M.A., 2003. Is methane venting at the seafloor recorded by $\delta^{13}C$ of benthic foraminifera shells? Paleoceanography 18, 1062.

Trudinger, C.M., Enting, I.G., Etheridge, D.M., Francey, R.J., Levchenko, V.A., Steele, L.P., Raynaud, D., Arnaud, L., 1997. Modeling air movement and bubble trapping in firn. J. Geophys. Res. 102, 6747–6763.

Uchida, M., Ohkushi, K., Kimoto, K., Inagaki, F., Ishimura, T., Tsunogai, U., TuZino, T., Shibata, Y., 2008. Radiocarbon-based carbon source quantification of anomalous isotopic foraminifera in last glacial sediments in the western North Pacific. Geochem. Geophys. Geosyst. 9, Q04N14.

Valdes, P.J., Beerling, D.J., Johnson, C.E., 2005. The ice age methane budget. Geophys. Res. Lett. 32, L02704.

Wang, W.-C., Shi, G.-Y., Kiehl, J.T., 1991. Incorporation of the thermal radiative effect of CH_4, N_2O, CF_2Cl_2, and $CFCl_3$ into the National Center for Atmospheric Research community climate model. J. Geophys. Res. 96, 9097–9103.

Weber, S.L., Drury, A.J., Toonen, W.H.J., van Weele, M., 2010. Wetland methane emissions during the last glacial maximum estimated from PMIP2 simulations: climate, vegetation, and geographic controls. J. Geophys. Res. 115, D06111.

Wilkinson, M.J., Monson, R.K., Trahan, N., Lee, S., Brown, E., Jackson, R.B., Polleys, H.W., Fay, P.A., Fall, R., 2009. Leaf isoprene emission rate as a function of atmospheric CO_2 concentration. Global Change Biol. 15, 1189–1200.

Witrant, E., Martinerie, P., Hogan, C., Laube, J.C., Kawamura, K., Capron, E., Montzka, S.A., Dlugokencky, E.J., Etheridge, D., Blunier, T., Sturges, W.T., 2011. A new multi-gas constrained model of trace gas non-homogeneous transport in firn: evaluation and behavior at eleven polar sites. Atmos. Chem. Phys. Discuss. 11, 23029–23080.

Zeebe, R.E., 2007. Modeling CO_2 chemistry, $\delta^{13}C$, and oxidation of organic carbon and methane in sediment porewater: implications for paleo-proxies in benthic foraminifera. Geochim. Cosmochim. Acta 71, 3238–3256.